

SHC 2012

Experimental and two-dimensional numerical simulation of an unglazed transpired solar air collector

Messaoud Badache^a, Daniel Rousse^a, Stéphane Hallé^a,
Guillermo Quesada^{a*}, Yvan Dutil^a

^a*Technologies of energy and energy efficiency industrial research chair (t3e),
École de technologie supérieure, Université du Québec
1100, Notre-Dame St. West, Montreal, H3C 1K3, Canada*

Abstract

In this paper, the thermal efficiency of a solar air collector called unglazed transpired collector (UTC) has been investigated both experimentally and numerically (CFD). Experimental measurements included the following variables: the temperatures of the air entering and leaving the UTC for three air mass fluxes, three distinct irradiations and two plenums thicknesses. A commercial finite volume software (Fluent) was used to model the heat transfer through the UTC. Turbulent effects were modelled by the RNG $k-\epsilon$ turbulence model. It was found that a weak heat exchange process mainly took place at the plenum; the maximum efficiency differences expected between the two plenums widths (5 and 15 cm) was 2.85%.

© 2012 The Authors. Published by Elsevier Ltd. Open access under [CC BY-NC-ND license](http://creativecommons.org/licenses/by-nc-nd/3.0/).
Selection and/or peer-review under responsibility of PSE AG

Keywords: CFD, Turbulence, unglazed transpired solar air collector, Thermal performance

1. Introduction

Unglazed transpired collectors (UTC's) are now a well-recognized solar air heater for heating outside air directly [1]. They are key components in many engineering applications, such as in institutional and residential heating, industrial processes like sewage wastewater treatment, and food processing. They differ from conventional solar air collectors in that their external wall is replaced by a black perforated sheet, i.e. unglazed, that allows the collection of solar irradiation.

* Corresponding author. Tel.: +0-000-000-0000 ; fax: +0-000-000-0000 .
E-mail address: guillermo@t3e.info.

The earlier studies carried out on UTCs showed that modelling a full-scale UTC at this time required some simplifications to fit the numerical model within the limits of the computer resources [2]. Cao et al. [3] showed that modelling the flow around even a single hole requires several hours computer time. Indeed two main approaches were explored, one was to include only the plenum region [2], the second approach use's symmetry of the system (perforated plate) in which simulations were restricted to the perforations region[1, 3-5]. Therefore no detailed studies have yet-been undertaken of the thermal performances of the whole collector including the plenum and the perforations. Hence, the purpose of the present investigation is to enrich the knowledge already acquired on UTC's by performing an experimental and numerical simulation of a two-dimensional unglazed transpired collector including the plenum and the perforations regions.

Nomenclature

A_{coll}	collector area (m^2)
b	slot's thickness (mm)
G_0	volumetric heat generation (W/m^3)
G_T	absorbed irradiation intercity (W/m^2)
H	absorber plate height (cm)
L	pitch of between slots (mm)
\dot{m}	air mass flux ($kg/s \cdot m^2$)
T_{amb}	ambient air temperature ($^{\circ}C$)
T_{out}	outlet air temperature ($^{\circ}C$)
w	plenum thickness (cm) Greek symbols
α	absorption coefficient
ε	turbulent dissipation rate (m^2/s^3)
η_{coll}	collector efficiency
λ	thermal conductivity ($W/m \cdot K$)
ρ_{air}	air density (kg/m^3)
δ_{ij}	Kronecker delta

In this paper the thermal performances of an UTC are investigated both experimentally and with computational fluid dynamics (CFD). Experimental investigations were carried out in a laboratory with controlled environment. Measurements included the ambient and outlet air temperatures, and air mass flow rate through the UTC for two plenums thicknesses and three distinct irradiations. The plate's perforations were chosen to be slits to enable the comparison with 2D numerical simulations. The commercial software (Fluent) was used that solves the Reynolds–Average Navier–Stokes Equations (RANS) coupled with energy conservation and turbulence modeling. The low-Reynolds RNG $k-\varepsilon$ turbulence model has been employed to simulate the turbulent cases. The Boussinesq approximation was used to account for the density variation within the collector.

2. Experimental method

Two UTCs prototypes have been built, instrumented and tested in laboratory conditions. These will be designated as “w-5” (plenum of 5 cm) and “w-15” (plenum of 15 cm). Each comprising, a vertical wooden box, an absorber plate, an air gap with thickness (w) which is the back wall to plate spacing (plenum). The air leaves the plenum via the top back wall. The sides and the back of the collector are insulated to minimise heat losses and to act as adiabatic walls, while the front face was exposed to lamps irradiation and ambient temperature. A vertical section of the UTC prototype studied is shown in Fig 1. Note that the air suction system and the artificial source of irradiation are not shown on Fig 1.

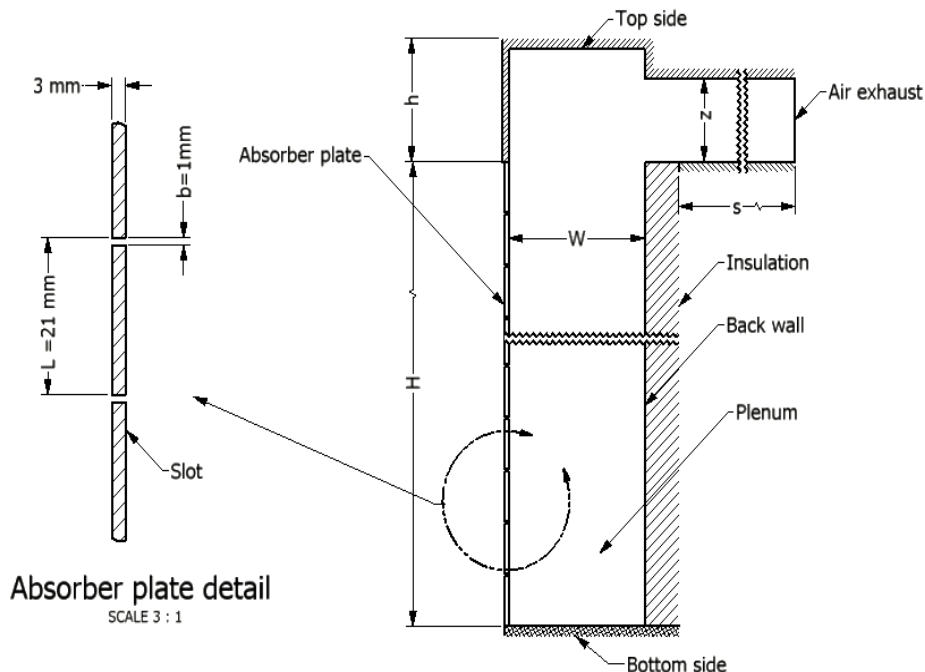


Fig. 1. Vertical section of the UTC showing the geometry studied

The absorber test plate consists of a black painted aluminum sheet ($\lambda = 202\text{ W/m}\cdot\text{K}$) mounted on the front face of the wooden box, and has the same dimensions in all tests; 0.3 cm thick, 0.48 cm height (H) and 36 cm width (not visible in the 2D model). It includes an equally spaced single row of slots (21 slots), of width (b) 1 mm thick uniformly spaced at a distance (L) of 21 mm, through which air is drawn. This is equivalent to an apparent surface of 0.174 m^2 and to about 5% porosity.

Air is drawn by 75.5 L/s inline duct ventilator (DB206), and emerges the collector at the rear box through (z) a 10 cm fitting reducer. The air mass flow rate in the collector was controlled by a variable speed drive model (3PN116B, 110/120 V, 60Hz) which allows the adjustment (control) of three mass flux required in the experiments ($0.0133, 0.0266, 0.0411\text{ kg/s}\cdot\text{m}^2$).

Tests were performed for 3 levels of irradiation ($300, 450$ and 600 W/m^2) with an artificial solar simulator, which involves 28 globe®- projectors with T3/J-TYPE/87 mm, 150 Watts, light bulbs that collectively provide a total radiative intensity of 4.2 kW.

For each plenum thicknesses (5 cm and 15 cm) three irradiations levels (300, 450 and 600 W/m²) and three mass fluxes (0.0133, 0.0266, 0.041 kg/s·m²) were studied. In total 18 test runs were performed. Each test started by adjusting the irradiation level and the mass flow rate. After, the readings (T_{amb} and T_{out}) were recorded. All readings are noted once the steady-state conditions are reached. The steady state for each run was attained generally within 2–2.5 h. Fifteen calibrated (0.2 mm diameter) k-type thermocouples (with accuracy 0.3 °C) have been used for the measurement of temperature, at different points of the test apparatus. The temperature recording was carried out using a central data acquisition (National Instrument-USA, SCXI-1000), carried out to record temperatures at fixed time interval of 1 second.

The UTC efficiency (η_{coll}) was estimated from an energy ratio transfers, i.e. from the ratio of the useful heat gain delivered by the collector divided by the incident irradiation on the collector surface. UTC's efficiency can be determined by the following equation (1):

$$\eta_{coll} = \frac{\dot{m}c_p(T_{out} - T_{amb})}{G_T} \quad (1)$$

3. Numerical method

3.1. Physical Problem and turbulence modeling

Two UTC models were built with two different plenum thicknesses (5 and 15 cm). The numerical models were designed to resemble the essential features of the experimental prototype. Indeed, the considered geometry corresponds exactly to the one employed in the experiments (Fig 1). An outer domain (exterior) was added bounded by the inlet air section (at plan x_{in} , see Fig 2 (b)). Although the three modes of heat transfer in the UTC are present, radiation heat exchange between the absorber plate and the back wall and between the absorber plate and the surroundings has been considered negligible as suggested by [6]. The flow is assumed to be steady, turbulent and two-dimensional. The Boussinesq approximation was used to account for the density variation. This approximation is valid since the temperature differences in the domain were typically less than 32 °C. The thermophysical properties of the fluid are evaluated at a reference temperature (evaluated from experimental measurements) and assumed to be constant, except the buoyancy term. For brevity the mathematical model is not listed here, full equation sets and details (k , ε , ν_t , Pr_t , and S_{ij}) for this model are available in [7].

The assumption of turbulent flow was justified in two ways. First, the presence of slots changes the flow behavior over the absorber plate, and typically creates turbulent recirculation regions in the plenum. Second, the fluid dynamic models representative of the air motion inside the plenum shows rather complex results, involving turbulent and laminar flows [2]. The flow may be laminar or turbulent, depending on the region and the air flow rate through the collector. Apart from the intrinsic difficulty to defining the region of the collector where the flow is laminar or turbulent, it is impossible to apply both laminar and turbulent models to the same computational model. To check a merging between the laminar and turbulent flow a turbulent model seems to be more appropriate in this situation, indeed the Reynolds–Normalized Group (RNG) k- ε model derived by Orszag et al. [8] has been used. This model was recommended in literature [9] and further in [10] for predicting air motion in enclosed airflow simulations.

3.2. Mesh design and boundary conditions

A structured mesh grid is used inside the slot, the solid region (absorber plate), and at a region $x = \pm 1$ cm from the absorber plate (i.e. 1 cm upstream and 1 cm downstream of the plate). A large number

of grid points are placed inside the slots where the temperature and velocity gradients are expected to be significant, and at geometrically decreasing distances in the regions next to the solids regions. A coarse non structured mesh grid was used within the rest of the domain since the flow in these regions is relatively quiet. The same method was used for both plenum cases (5 cm and 15 cm). Fig 2 (a), shows the grid topology near a slot. Table 1, shows the characteristics of the three mesh (A, B and C) studied for each plenum case, subscript N_a , N_b , N_c , and N_d represent the number of nodes at the edges of the smallest repeating pattern as shown in Fig 2 (a), while N_t , C_L represent the total number of nodes and cells within the whole computational domain.

Table 1. Grid parameters for the two plenums configuration

		C_L	N_t	N_a	N_b	N_c	N_d
Plenum (w-5)	Mesh A-5	100494	67125	10	5	15	25
	Mesh B-5	168699	112997	15	10	20	30
	Mesh C-5	180342	126025	30	20	20	30
Plenum (w-15)	Mesh A-15	172961	103319	10	5	15	25
	Mesh B-15	282615	220351	15	10	20	30
	Mesh C-15	393026	237281	30	20	20	30

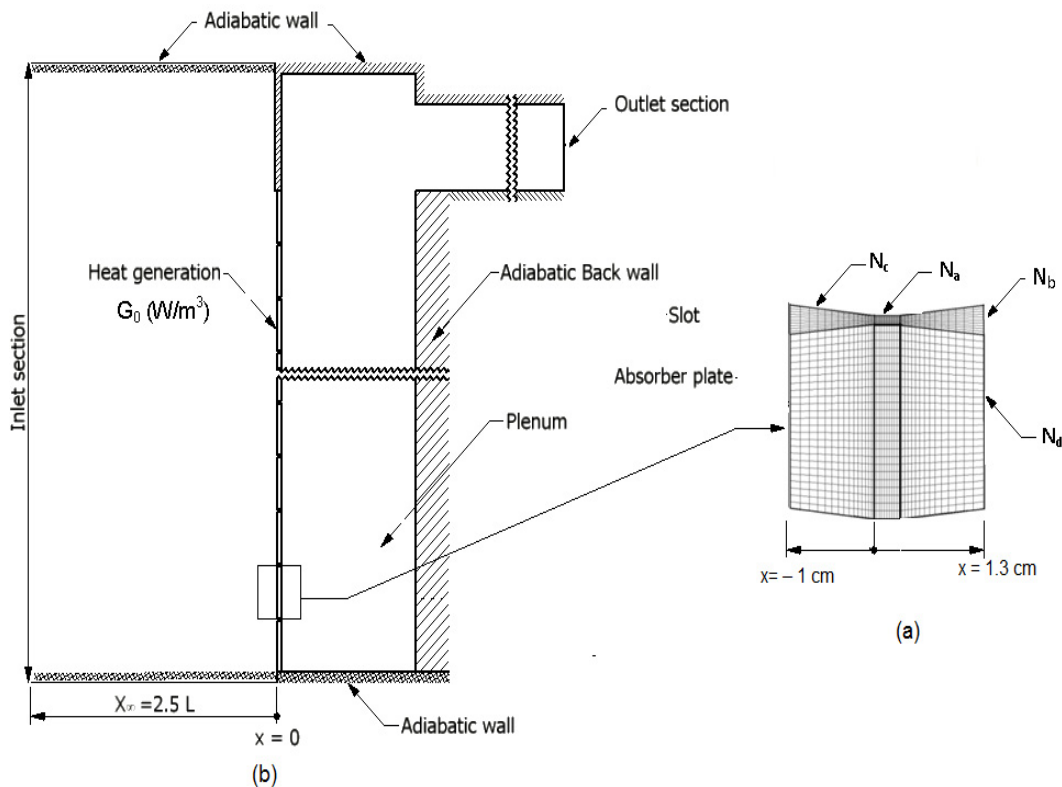


Fig. 2. (a) Grid topology near a slot and one spacing L of the plate; (b) boundary conditions imposed on the computational domain

Fig 2 (b) shows the boundary conditions imposed on the computational domain. Initial and boundary conditions were set as close as possible to the experimental conditions. Three types of boundary conditions were considered.

At walls: the no-slip boundary conditions have been considered on all of the rigid walls. In all cases, vertical (back wall) and horizontal (bottom, top) walls have been considered as adiabatic. At the absorber plate, a volumetric heat generation term was specified (G_0 , equal to 2×10^5 , 1.5×10^5 , 1×10^5 W/m³) equivalent to absorbed solar radiation ($\alpha \cdot G_T$, equal to 600, 450, 300 W/m²).

At the outlet air section: a negative inlet velocity condition was imposed since the experimental mass fluxes through the UTC are known.

At the inlet air section: on the left outside of the plate (i.e. at the distance $x \rightarrow \infty$) the computational domain is bounded by a free air stream inlet with an assumed total pressure of 0 Pa. The incoming air temperature was specified to be equal to the ambient temperature T_{amb} .

3.3. Numerical methodology and grid independence study

The set of governing coupled non-linear differential equations have been solved numerically via Fluent which is based on a finite volume procedure. Convective and diffusive terms are discretized with a second order upwind scheme. The SIMPLE algorithm of Patankar and Spalding [11] was used for the velocity-pressure coupling. The solution was considered to be converged when the residuals were on the order of 10^{-6} for continuity, momentum, turbulence quantities and 10^{-10} for energy. All simulations were performed on a i7 processors, 2.13 GHz and 12 GB of memory.

A grid dependence study was carried out (for the two plenum configurations) to ascertain the accuracy of the numerical results and to decide what grid size (N_t) will be used for all the simulations. The efficiency of the UTC was the relevant parameter to be analyzed. The simulation case with mass fluxes 0.0411 kg/s·m² and irradiation intensity level 600 W/m² was considered in the grid independence study, since this case was the most restrictive in terms of convergence compared to the other cases.

The Grid Convergence Index (GCI) method, recommended by the Fluids Engineering Division of ASME for discretization error estimation was used in the present study, which is based on the Richardson extrapolation [12]. The parameters of the different meshes and the corresponding computed value of efficiency used in the GCI study are illustrated in Table 2, where C_{Li} and η_{coll-i} denotes respectively the total number of cells used and the efficiency solution on the i th mesh grid.

Table 2. Calculation results of discretization error

Calculated parameters	Plenum (w-5)	Plenum (w-15)
CL1, CL2, CL3	100494, 168699, 180342	172961, 377774, 393026
η_{coll-1}	0.901	0.913
η_{coll-2}	0.879	0.875
η_{coll-3}	0.875	0.866
$\eta_{coll-(R-ext)}$	0.873	0.861
GCI	0.37%	0.84%

According to Table 2, the numerical uncertainty in the fine-grid solution for the cases of (w-5) and (w-15) are 0.37% and 0.84% respectively, and the extrapolated values for the efficiency (estimated as the number of cells approached infinity) are 87.27% and 86.07%. From a viewpoint of grid solution convergence, the difference between extrapolated and fine mesh is negligible. For this reason, the

Richardson extrapolated solution $\eta_{\text{coll-(R-ext)}}$ for each plenum case cannot be differentiated from the fine grid solution. In summary, the results that will be presented in the subsequent simulations were calculated using mesh grid (C-5) for plenum (w -5) and (C-15) for plenum (w -15) with y^+ less than unity ($0.5 < y^+ < 0.8$).

4. Results

A series of numerical simulations were performed to investigate the thermal performance of the UTC, under k - ϵ RNG model. The numerical results are presented below in terms of the collector efficiency then compared to experimental test data. Results are obtained at three air mass fluxes (0.0133, 0.0266, 0.0411 $\text{kg/s}\cdot\text{m}^2$), three irradiation levels $G_T = 600$; 450; and 300 W/m^2 and two plenum thicknesses ($w = 5$ cm and 15 cm). The effect of plenum thickness is also considered on the thermal behavior of the UTC.

4.1. Comparison with experimental results

Data related to the instrumentation used in this study stated that the measurement of flow velocity and irradiation have an uncertainty of $\pm 3\%$ and $\pm 1\%$ respectively. The uncertainty in the temperature measurement was ± 0.3 °C. The maximum value for the uncertainty on the efficiency results is $\pm 5.4\%$.

The comparison between CFD simulations and the experimental efficiency measurements for the two plenum thicknesses was performed for three irradiation levels (300, 450 and 600 W/m^2). For brevity only case with irradiation level of 300 and 600 W/m^2 are represented her (Fig 3 (a) and (b)).

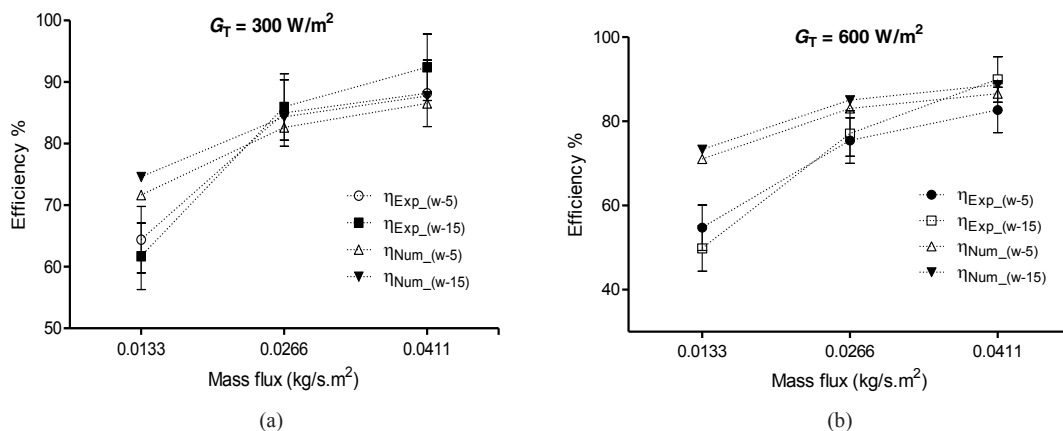


Fig. 3. Comparison of the computed and measured efficiency; (a) $G_T = 300 \text{ W/m}^2$; (b) $G_T = 600 \text{ W/m}^2$

Globally, Fig 3 (a) and (b) show that the predicted efficiency was within the experimentally measured efficiency uncertainty range for almost all of the measured points. However, the experimental data obtained at the lowest mass fluxes and high irradiation level shows a slight disagreement with the model predictions. This disagreement is most likely due to the fact that there are unknown experimental inputs such as turbulence intensity, and radiative heat loss from the absorber plate to the surroundings, which were not accounted for in the model simulations. These losses by radiation are significant at low mass flux and high irradiation levels.

4.2. Effect of mass fluxes

One of the parameters that were used to control the thermal performance of the UTC is the mass flux, defined as the mass flow rate per unit collector area. Fig 4 (a) shows the variations of the thermal efficiency of the UTC with air mass flux for three irradiation levels and two plenum cases. The thermal efficiency of the UTC was calculated as in equation 1. It can be found in Fig 4 that the efficiency increases with increasing air mass fluxes, for the two plenum cases. This is because the heat transfer capacity depends directly on the mass flux, which induces higher velocities through the slots and more heat transfer from the absorber plate to the air.

Initially, the computed efficiency rises, rapidly at low mass flux, (by about 11% between 0.0113 and 0.0266 kg/s·m²), but only slightly (about 3.5%) at mass flux above 0.0266 kg/s·m². These trends are generally consistent with the results reported by [13] and [14]. Which have noted that the efficiency is nearly constant for approach velocities greater than 0.05 and 0.04 m/s, equivalent to about 0.042 and 0.034 kg/s·m².

4.3. Effect of irradiation

Fig 4 (b) illustrates the variation of the UTC air temperature rise ($T_{out} - T_{amb}$) with air mass flux for different levels of incident irradiation and two plenum cases. As with any solar collector, for a constant irradiation level, air temperature rises tend to decrease with increasing mass flux. In addition, at higher irradiation levels, the mass flux has a greater effect on the air temperature rise since there is more thermal energy ($\alpha \cdot G_T \cdot A_{coll}$) available to the sucked air. For example of plenum (w-15), when the mass flux increases from 0.0133 to 0.0411 kg/s·m², the air temperature rise drops by 18.84°C for 600 W/m² of irradiation compared to only 9.76°C for an irradiation level of 300 W/m², which is nearly double. Note, that the air temperature rise drop rapidly initially but shows less diminishing returns at higher mass fluxes. In addition, for a constant mass flux, the air temperature rise tends to increase with increasing irradiation level, which is quite logical and is true for both plenum cases.

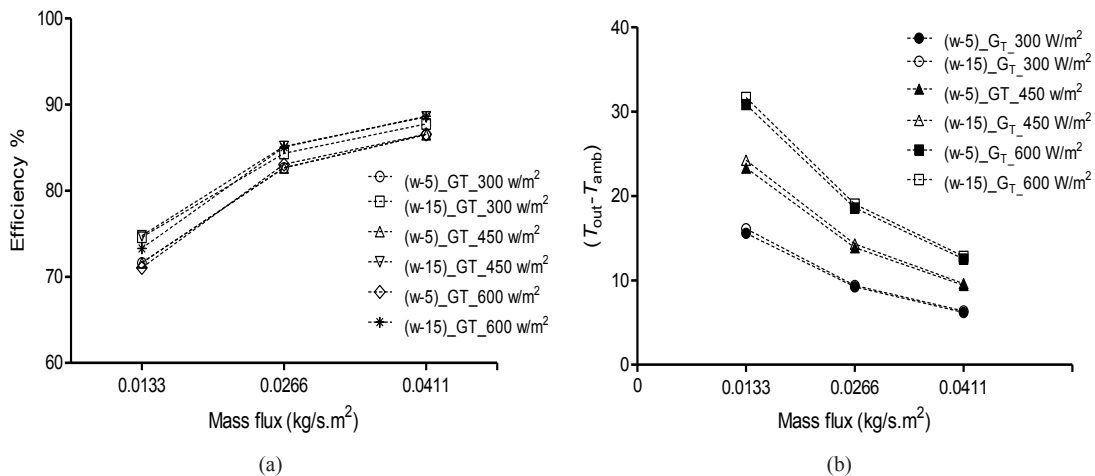


Fig. 4. (a) Efficiency vs. mass fluxes for two plenum cases; (b) computed air temperature rise for different levels of irradiation

Although the numerical results, indicate that efficiency increases, with the increase of the air mass fluxes. The experimental results show a small decrease in efficiency as the irradiation intensity increases

(from 300 to 600 W/m²) for both plenum thicknesses. This increase is more pronounced especially at high irradiation level and low mass fluxes. Nevertheless, this decreasing trend from the current results may be due to a relatively high absorber temperature, and the low capacity of air at moderate mass flux to extract all available collector thermal energy. This increases the heat losses from the absorber plate to ambient air and, results in a decrease in the thermal efficiency of the UTC. Hence to minimize heat losses from the UTC and to maximize collector efficiency, it is necessary to operate the collector at medium or high mass fluxes whatever the irradiation conditions.

4.4. Effect of plenum thickness

In order to compare the plenum's effect to the efficiency, the plenum thicknesses (w), was varied between 5 cm and 15 cm. The simulation results for the two different options are given in Fig 4 (a). This figure shows a slight influence of plenum thickness on collector efficiency. The efficiency is clustered in two groups at plenum thickness 5 cm and 15 cm. The percent differences of the efficiency between the two plenum cases (5 and 15 cm) varied from 1.92 and 2.85%. This slight difference of efficiency compare favorably to the experimental results except in case of low mass flux (0.0133 kg/s·m²) and agree with studies done in [15].

In the present study the effect of plenum thickness on the efficiency is low compared to the effect of mass flux and irradiation. For a complete study of plenum thickness effects on the UTC efficiency, one must examine the absorber plate upstream and downstream flow and the heat transfer process. On one hand with an adiabatic back wall, all the heat collected by the absorber plate surface is transferred into the air stream, and therefore 100% of the heat exchange process took place at the absorber plate. In addition, downstream of each jet slots, a recirculation zone develops, and the cumulative flow through the plenum increases due to the upstream jets. On the other hand, the fluid motion and heat transfer at the outward face of the absorber plate is the same regardless the plenum thickness. Therefore the efficiency difference expected between the two plenum cases can only be due to the heat transfer occurs at the back side of the absorber plate. A slight difference in efficiency is expected because the majority of the heat transfer occurs at the outward face of the absorber plate for both plenum thicknesses.

5. Conclusion

The thermal efficiency of a UTC has been investigated both experimentally and numerically (CFD). Experimental measurements included the following variables: the air temperatures entering and leaving the UTC for three air mass flow rates, three distinct irradiations and two plenums thicknesses. It can be found from the study that:

- The efficiency increases with increasing air mass fluxes for the two plenum cases. This is because the heat transfer capacity depends directly on the mass flow rate, which induces higher velocities through the perforations and more heat transfer from the plate to the air.
- Increasing the irradiation level seems to have a very limited effect on the collector efficiency for both plenum. Still, the experimental results show a small increase in efficiency as the irradiation intensity decreases (from 600 to 300 W/m²) for both plenum thicknesses. Nevertheless, this small effect may be due to the reduction of the absorber plate temperature, resulting in lower losses from the collector at low irradiation.
- A slight influence of plenum thickness' on collector efficiency, the percent differences of the efficiency between the two plenum cases varied from 1.92 and 2.85%. This slight dependence of UTC efficiency compare favorably to the experimental results except in the case of low mass flux (0.0133 kg/s·m²).

Acknowledgements

This work was supported by the t3e industrial research chair and its financial partners; the authors would like to acknowledge their invaluable contributions.

References

- [1] Arulanandam, S.J., K.G.T. Hollands, and E. Brundrett, A CFD heat transfer analysis of the transpired solar collector under no-wind conditions. *Solar Energy*, 1999; 67(1-3): 93–100
- [2] Gunnewiek, L.H., E. Brundrett, and K.G.T. Hollands, Flow distribution in unglazed transpired plate solar air heaters of large area. *Solar Energy*, 1996;58(4–6): 227–237.
- [3] Cao, S., K. Hollands, and E. Brundrett. Heat exchange effectiveness of unglazed transpired-plate solar collector in 2D flow. 1993.
- [4] Kutscher, An investigation of heat transfer for air flow through low porosity perforated plates, 1992, university of colorado: Boulder. p. 250.
- [5] Gawlik, K., C. Christensen, and C. Kutscher, A Numerical and Experimental Investigation of Low-conductivity Unglazed, Transpired Solar Air Heaters. *Journal of Solar Energy Engineering*, 2005; 127(1): 153–155.
- [6] Gawlik, K. and C. Kutscher, A Numerical and Experimental Investigation of Low-Conductivity Unglazed, Transpired Solar Air Heaters. ASME Conference Proceedings, 2002.(16893): 47–55.
- [7] Zamora, B. and A. Kaiser, Thermal and dynamic optimization of the convective flow in Trombe Wall shaped channels by numerical investigation. *Journal of Heat and Mass Transfer*, 2009;45(11): 1393–1407.
- [8] Orszag, S.A., et al., Renormalization group modeling and turbulence simulations. Near-wall turbulent flows, Proceedings of the International Conference, Tempe, AZ; Elsevier Science Publishers, Amsterdam ,1993;1031–1046.
- [9] Fuliotto, R., et al., Experimental and numerical analysis of heat transfer and airflow on an interactive building facade. *Energy and Buildings*, 2010;42(1):23–28.
- [10] Zhang, Z., et al., Evaluation of various turbulence models in predicting airflow and turbulence in enclosed environments by CFD: Part 2—Comparison with experimental data from literature. *HVAC&R Research*, 2007; 13(6): 871–886.
- [11] Patankar, S.V. and D.B. Spalding, A calculation procedure for heat, mass and momentum transfer in three-dimensional parabolic flows. *International Journal of Heat and Mass Transfer*, 1972; 15(10):1787–1806.
- [12] Celik, I.B., Ghia, U., Roache, P. J., Freitas, C. J., Coleman, H., and Raad, P. E., Procedure for Estimation and Reporting of Uncertainty Due to Discretization in CFD Applications. *Journal of Fluids Engineering*, 2008;130(7): 078001.
- [13] Kutscher, C.F., C.B. Christensen, and G.M. Barker, Unglazed transpired solar collectors: heat loss theory. *Journal of Solar Energy Engineering*, Transactions of the ASME, 1993;115(3):182–188.
- [14] Leon, M.A. and S. Kumar, Mathematical modeling and thermal performance analysis of unglazed transpired solar collectors. *Solar Energy*, 2007;81(1): 62–75.
- [15] Biona, J. and A. Culaba, Performance Curve Generation of an Unglazed Transpired Collector System for Solar Crop/Fish Drying, 2002, M. Sc. Thesis, De La Salle University, Manila.